Effect of Interfacial Engineering in Solid-State Nanostructured Sb_2S_3 Heterojunction Solar Cells

*Takafumi Fukumoto, Thomas Moehl, Yusuke Niwa, Md. K. Nazeeruddin, Michael Grätzel, and Lioz Etgar**

It has been recognized that solar energy is one of the promising sources of renewable energy to power our planet, and to industrialize this technology requires low-cost and high performance. Recently dye-sensitized solar cells (DSSC)[1,2] based on nanoporous TiO_2 electrode achieved high power conversion efficiency exceeding 12.3%.[3] However, since DSSC was based on liquid-electrolyte, the cell requires organic solvent leakage proof sealants that are rather expensive. In order to address those problems, several research groups are focused on the solid electrolyte such as Spiro- MeOTAD,[4,5] CuSCN,[6] and P3HT.[7] In place of the dyes, inorganic semiconductor quantum dots (QDs) or extremely thin absorber (ETA) such as PbS,[8,9] CdS,[10] CdSe,[11–14] CdTe,[15] $CuInS_2$,[16] $Cu_{2-x}S$,[17] and Sb_2S_3 have been investigated. Those inorganic semiconductors may offer several benefits due to their excellent optical properties,[18] large excitonic dipole moments[19] and high extinction coefficients.[20]

Sb_2S_3 has been investigated as a sensitizer in heterojunction solar cells by several researchers[21–28] due to its suitable band gap of 1.7–1.8 eV and high absorption coefficient (1.8×10^5 cm^{-1} at 450 nm).[29] However the Sb_2S_3 heterojunction solar cell still suffers from much recombination mainly because of the back reaction at the TiO_2/hole conductor interface.[23]

There are several strategies to suppress recombination; in DSSC, higher band gap materials such as MgO,[30] Nb_2O_5,[31] SiO_2,[32] ZnO,[33] and ZrO_2[34] were used as blocking layers at the interface between the TiO_2 and the electrolyte. The use of Al_2O_3 as a blocking layer in ETA cells with Sb_2S_3 as absorber and CuSCN as hole conductor was demonstrated, achieving 3.7% power conversion efficiency. The physical separation of injected electrons was improved as a result of this blocking layer in the ETA cell.[35] Another possibility to inhibit recombination is through a surface treatment of the absorber or the TiO_2. Surface treatment in Sb_2S_3 inorganic–organic solar cell was demonstrated using Mg^{2+}, Ba^{2+}, and Al^{3+} which results in an increase in the power conversion efficiency by 8% for Al^{3+}, 14% for Mg^{2+} and 24% for Ba^{2+}.[36] The use of co-adsorption in DSSC has also been used; for example, hexadecylmalonic acid (HDMA),[37] 1-decyl phosphonic acid (DPA)[38] and 3-phenylpropionic acid (PPA)[39] have been co-adsorbed along with sensitizer onto nanocrystalline TiO_2 film. Co-grafting of the two amphiphiles results in the formation of mixed monolayer which should be more tightly packed than when the sensitizer is adsorbed alone, providing a more effective insulated barrier for the back electron transfers from TiO_2 conduction band to triiodide electrolyte.[37–39]

Here we report the surface treatment by DPA, which reduces the recombination and increases the open circuit voltage and the fill factor (FF) of the inorganic-organic heterojunction solar cell. The Sb_2S_3 was grown directly onto TiO_2 mesoporous electrodes using chemical bath deposition (CBD) followed by DPA treatment and covered by P3HT as hole transport material (HTM). We studied the effect of the DPA treatment by electrochemical impedance spectroscopy and reveal that the DPA treatment attaches to both surfaces, the uncovered TiO_2 surface and the Sb_2S_3 surface; as a result, it blocks the recombination inside this inorganic–organic solar cell.

Performance of the Sb_2S_3 heterojunction solar cells: **Figure 1**A shows a scheme of the device architecture. The bottom layer is composed of compact and mesocopic TiO_2 layers acting as blocking and electron collectors, respectively. Light is absorbed by the Sb_2S_3 while holes are transported by the P3HT, and collected at the Au counter electrode. It is important to note that the P3HT also absorbs light in addition to the Sb_2S_3. The energy level diagram of the Sb_2S_3 heterojunction solar cell is shown in Figure 1B; the conduction and valence bands of the Sb_2S_3 permit electron injection and hole transportation to the TiO_2 and to the P3HT, respectively.[40]

Figure 2(A) shows the cross section of the photovoltaic device; the FTO, the mesopores TiO_2 and the P3HT/PEOT:PSS can be observed. The energy-dispersive X-ray spectroscopy (EDX) shown in Figure 2(B) presents the elemental distribution through the cross section of the device. It can be observed that Sb and S are detected in the whole TiO_2 thickness, even close to the bottom of the TiO_2 layer. Therefore it can be concluded that Sb_2S_3 was penetrated into the mesopores TiO_2 film and its amount seems to be uniform for the whole TiO_2 thickness. Several dipping times were used, from 1 h up to 3 h; the optimum dipping time was found to be 2 h, which gave the best photovoltaic performance. However, it is obvious that, even at 2 h dipping, the surface of the mesopores TiO_2 was not covered completely by Sb_2S_3; basically, there is uncovered TiO_2

T. Fukumoto, Dr. Y. Niwa
Nissan Research Center
Nissan Motor Co., Ltd, Natsushima-cho, 1, Yokosuka, Kanagawa 237-8523, Japan
Dr. T. Moehl, Dr. Md. K. Nazeeruddin,
Prof. M. Grätzel, Dr. L. Etgar
Department of Sciences and Chemical Engineering
École Polytechnique Fédérale de Lausanne- EPFL, Lausanne, Switzerland
E-mail: lioz.etgar@epfl.ch
Dr. L. Etgar
Institute of Chemistry
The Hebrew University of Jerusalem
Jerusalem 91904, Israel

DOI: 10.1002/aenm.201200540

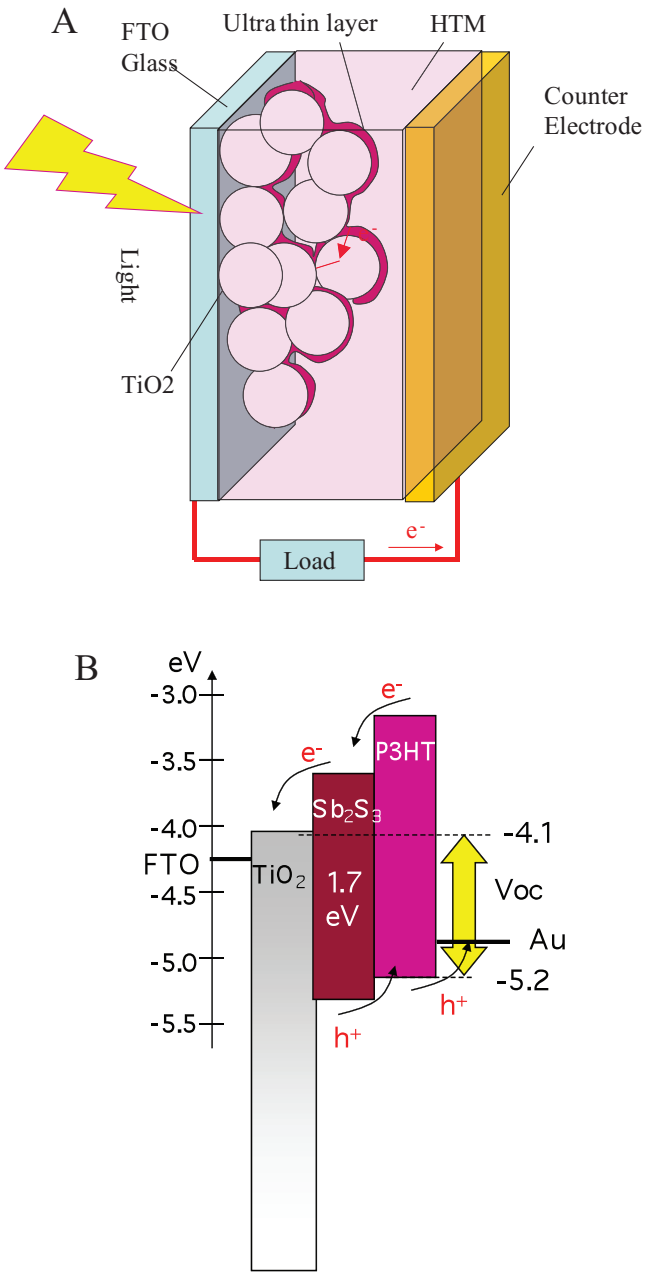

Figure 1. (A) Schematic illustration of the solar cell architecture; (B) energy level diagram of the inorganic-organic heterojunction solar cell. Energy level values were taken from Ref. [40].

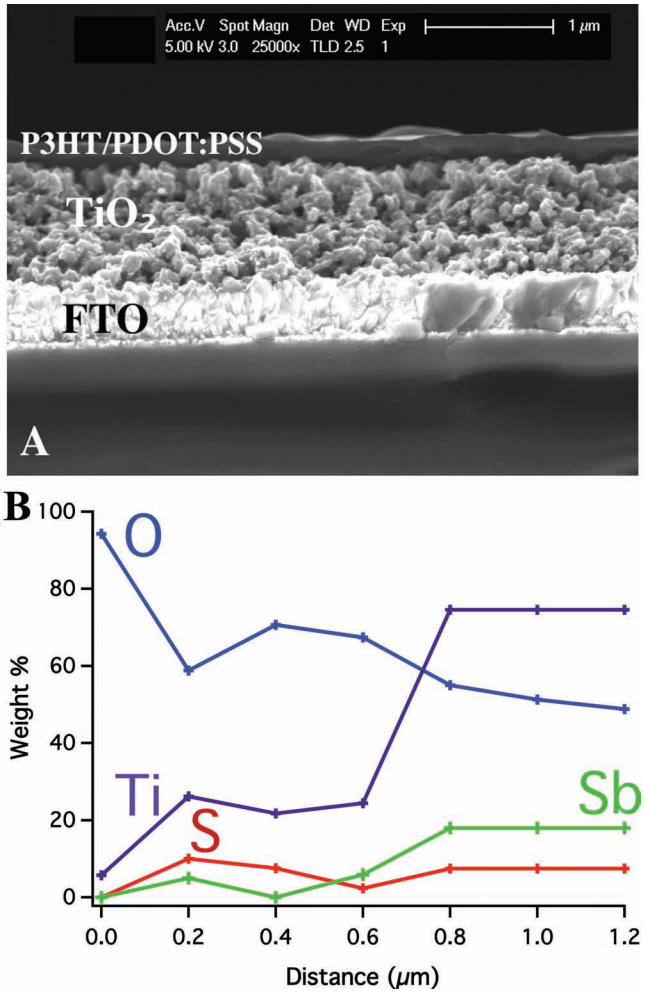

Figure 2. (A) Cross section of the Sb_2S_3 heterojunction solar cell; (B) EDX measurement; the elemental distribution through the cross section of the device can be observed.

surface, which can be in direct contact with the HTM (P3HT in this work). This direct contact can increase the recombination in the photovoltaic device.

In order to avoid this possible channel for recombination DPA treatment was introduced after the Sb_2S_3 deposition.

Figure 3A and **Table 1** show the *J–V* curves and the photovoltaic parameters. In the case of the cells without DPA treatment, a power conversion efficiency of 3.1% under 1 sun illumination with J_{sc} of 13.8 mA/cm^2, V_{oc} of 0.47 V, and FF of 0.48 has been obtained.

On the other hand, the performance of cells with DPA treatment was dramatically improved mainly due to the increase in V_{oc} and FF. A power conversion efficiency of 3.9% at 1 sun illumination has been obtained with J_{sc} of 14.2 mA/cm^2, V_{oc} of 0.51 V, and FF of 0.54.

Figure 3B shows the comparison of incident photon-to-current conversion efficiency (IPCE) of the cells with and without DPA treatment. The Sb_2S_3 heterojunction solar cell shows a good response in the visible through the 750 nm wavelength, the IPCE reaching its maximum of 86.5% at 400 nm while exceeding 80% in the range of 400–500 nm. A decrease can be seen at 600 nm, which is assumed to be due to attenuation of light caused by absorption of the P3HT film.[41] The band gap of the crystallite Sb_2S_3 can be estimated from the edge of the IPCE spectra, in this case it was equal to approximately 730 nm corresponding to 1.7 eV. Integration of the IPCE spectrum over the AM1.5 solar emission for the cells with DPA treatment yields a photocurrent density of 15.7 mA/cm^2 in good agreement with the measured value. In order to understand the reason for the

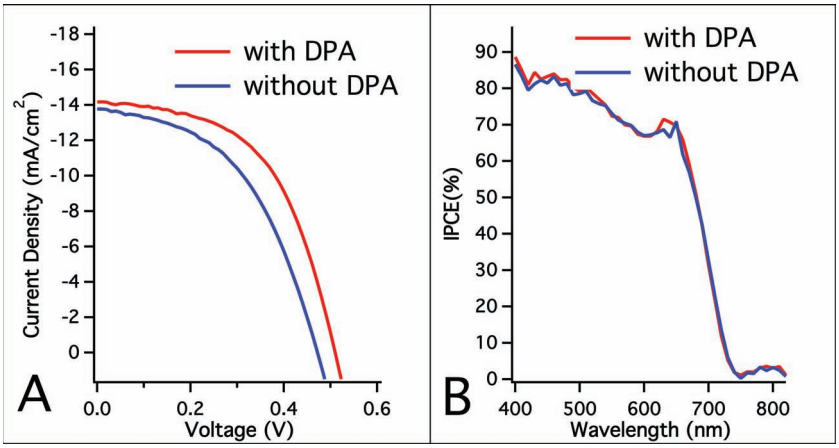

Figure 3. (A) Measured *J–V* characteristics for the Sb_2S_3 heterojunction solar cell. An aperture area of 0.15 cm^2 was placed over the device. (B) Spectral response curves of the photocurrent for the Sb_2S_3 heterojunction solar cell. The external quantum efficiency or incident photon to current conversion efficiency is plotted as a function of wavelength of the incident light.

Table 1. Photovoltaic parameters of cell with and without DPA treatment.

	η (%)	V_{OC} (mV)	J_{SC} (mA/cm^2)	FF
Without DPA	3.1	472	13.8	0.48
With DPA	3.9	510	14.2	0.54

improved photovoltaic performance due to the DPA treatment electrochemical impedance spectroscopy was preformed.

DPA treatment effect: In order to investigate the changes in the device performance by the DPA treatment, impedance spectroscopy (IS) was applied. Boix et al. published an electronic circuit model describing the type of investigated devices also presented in this publication. This model enables the determination of characteristic electronic parameters like the electron recombination resistance at the interface TiO_2/hole conductor (R_{CT}) or the chemical capacitance of the TiO_2 layer (C_μ).[23] **Figure 4** presents the change in dark current due to the treatment with DPA. The DPA treatment reduces the dark current which leads to the overall increased PCE, mostly by increasing V_{oc} and FF; see Table 1. Generally, two reasons can lead to such changes: the reduced recombination over the TiO_2/hole conductor interface or a shift in the conduction band of the TiO_2. From the literature it is known that DPA affects both the conduction band position and the recombinative behavior at the TiO_2/HTM.[42] The phosphonic acid binds strongly to the TiO_2 surface, building a barrier for the electron transfer between the mesoporous oxide and the redox electrolyte or HTM. With its electron withdrawing character DPA moves the conduction band to more positive energies. This normally leads to a reduction in V_{oc} but, on the other hand, the DPA treatment strongly retards recombination leading finally to an increase in V_{oc}. **Figure 5**A shows a typical result of R_{CT} and C_μ from the analysis of the impedance spectra. The R_{CT} shows clearly one of the reasons for the relatively low FF of the devices. Near 0 V, R_{CT} is dominated by the behavior of the interface of the compact TiO_2

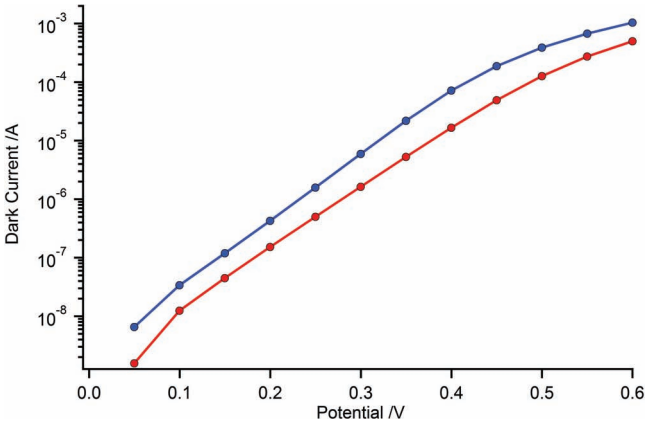

Figure 4. Dark current of the samples with (red) and without the DPA (blue) treatment.

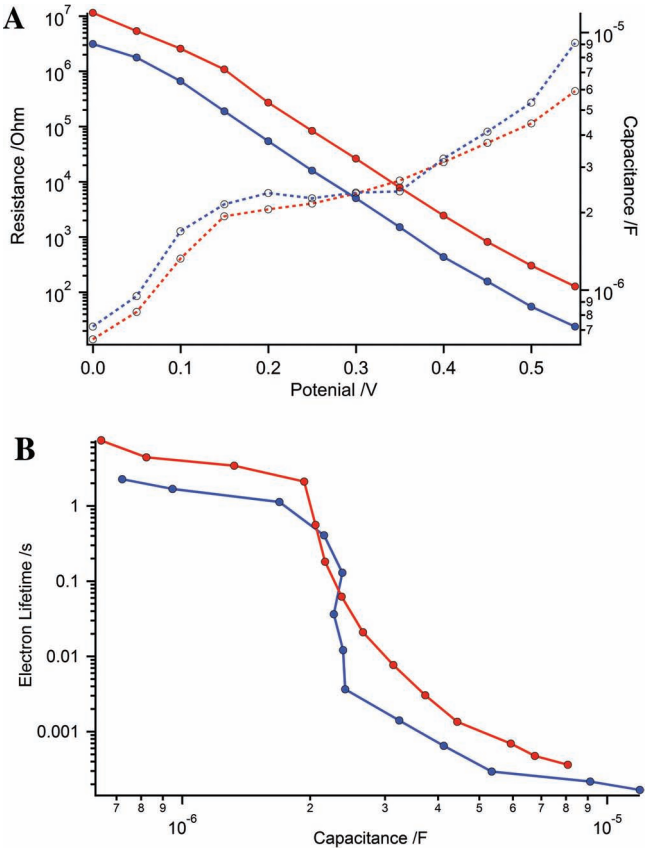

Figure 5. (A) R_{CT} (solid) and C_μ (dotted) from the IS measurements of the untreated (blue) and DPA treated (red) sample in the dark. (B) Electron lifetime in the dark.

blocking layer and the hole conductor. The resistance in this potential region decreases rapidly, indicating a shunted character (clearly also visible in the logarithmic dark current plot). After the DPA treatment, the devices show a decrease of the dark current and therefore an increase of R_{CT} can be observed. Also, a small shift in capacitance is visible. As mentioned above, the DPA treatment can also effect the conduction band position of the TiO_2 and not only the recombination resistance. Interestingly, the movement of the E_{CB} in the devices is opposite to the effect in liquid DSCs and much less pronounced.

Plotting the electron lifetime ($\tau_n = C_\mu \times R_{CT}$) against the capacitance (see Figure 5B), we can observe the lifetime in dependence of the amount of charge stored in the mesoporous film accounting for similar distance of the Fermi level (E_F) to the conduction band edge of the TiO_2. The lifetime for the DPA treated sample is longer. The difference is small but visible. It cannot be clearly determined which of the two effects, the reduction of the R_{CT} or the movement of the E_{CB}, is the main reason for the change in dark current although the recombination resistance change is probably the more weighted component.

The main contribution to the increase in FF and V_{OC} can be deduced from the IS analysis of the illuminated samples. The R_{CT} shows an increase in the DPA treated sample while the capacitance stays nearly unchanged (see **Figure 6**A). This shows that the change in conduction band position can only be a minor contribution to the gain in V_{OC} while the reduction of the recombination rate acts as the main effect in the increase of V_{OC}.

The lifetime of the electrons inside the TiO_2 is prolonged due to the pronounced increase in recombination resistance by the DPA treatment as visible in Figure 6B.

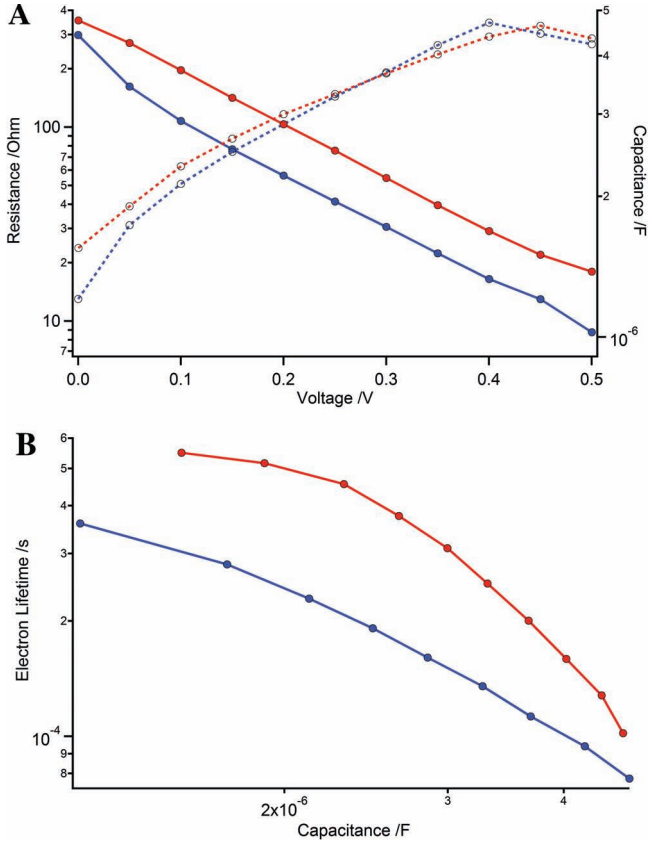

Figure 6. (A) R_{CT} (solid) and C_μ (dotted) from the IS measurements under illumination (untreated (blue) and DPA treated (red)). (B) Electron lifetime under illumination.

Conclusion

Influence of DPA surface treatment on the photovoltaic parameters was investigated. High efficiency solid-state nanostructured inorganic–organic heterojunction solar cell was presented. Sb_2S_3 was used as sensitizer grown by chemical-bath-deposition while P3HT was used as a hole conductor. It was observed that DPA treatment could improve the cell performance; impedance measurements showed that the increase in the cell performance and especially the increase in the V_{oc} and the FF were due to inhabitation of recombination. As a result, a power conversion efficiency of 3.9% at 1 sun illumination has been obtained reaching J_{sc} of 14.2 mA/cm^2, V_{oc} of 0.51 V, and FF of 0.54.

Experimental Section

Solar cell fabrication: Thin dense TiO_2 layer of ~100 nm thickness was deposited onto a SnO_2:F conducting glass substrate (15 Ω/cm, Pilkington) by spray pyrolysis method.[35] The deposition temperature of TiO_2 compact layer was 450 °C. Nanopores TiO_2 film (1 ~ 1.2 μm thick) was prepared by screen-printing method onto this substrate using 40 nm TiO_2 particles. The TiO_2 layer was annealed at 500 °C for 30 min in air. The substrate was immersed in 20 mM $TiCl_4$ aqueous solutions for 30 min at 70 °C and washed with distilled water and ethanol, followed by annealing at 500 °C for 30 min in air. The Sb_2S_3 layer was deposited by chemical bath deposition (CBD) with mixture solution of $SbCl_3$ and $Na_2S_2O_3$.[44] The as-deposited orange films of amorphous Sb_2S_3 were annealed at 300 °C for 30 min under N_2. After annealing, dark-brown crystalline stibnite Sb_2S_3 was removed from the oven immediately and cool down under N_2. The DPA treatment is similar to one previously reported,[28] but with slight modifications. The sample was immersed in 1 mM DPA ethanolic solution for 30 min followed by washing with acetonitrile. As an organic hole–transporting material (HTM), Poly-3-hexylthiophene (P3HT: Rieke metals) was used. The solution of the HTM (15 mg/mL in 1,2-dichlorobenzene) was spin-coated onto the Sb_2S_3/TiO_2 film with 2500 rpm for 60 s.[45] Then, in order to improve the contact between P3HT and Au a poly(3-4-ethylenedioxythiophene) doped with poly(4-stylenesulfonate) (PEDOT;PSS; Ossila 4083) diluted with two volumes of MeOH was spin-coated onto the P3HT/Sb_2S_3/TiO_2 at 2000 rpm for 30 s. The PEDOT:PSS/P3HT/Sb_2S_3/TiO_2 layer was annealed at 90 °C for 30 min under Ar. Finally the counter electrode was deposited by thermal evaporation of gold under a pressure of 5 × 10^{-5} Torr. The active area was 0.15 cm^2. After the preparation, the cells were allowed to expose in air and measured the next day.

Photovoltaic Characterization: Photovoltaic measurements employed an AM 1.5 solar simulator equipped with a 450W Xenon lamp (Model No. 81172, Oriel). Its power output was adjusted to match AM 1.5 global sunlight (100 mW/cm^2) by using a reference Si photodiode equipped with an IR-cutoff filter (KG-3, Schott) in order to reduce the mismatch between the simulated light and AM 1.5 (in the region of 350–750 nm) to less than 2% with measurements verified at two PV calibration laboratories (ISE (Germany), NREL (USA)). *I–V* curves were obtained by applying an external bias to the cell and measuring the generated photocurrent with a Keithley model 2400 digital source meter. The voltage step and delay

time of photocurrent were 10 mV and 40 ms, respectively. A similar data acquisition system was used to determine the monochromatic incident photon- to-electric current conversion efficiency. Under full computer control, light from a 300 W Xenon lamp (ILC Technology, U. S. A.) was focused through a Gemini-180 double monochromator (Jobin Yvon Ltd., U. K.) onto the photovoltaic cell under test. The monochromator was incremented through the visible spectrum to generate the IPCE (λ) as defined by IPCE (λ)) = 12400(Jsc/$\lambda\varphi$), where λ is the wavelength, Jsc is short-circuit photocurrent density (mA cm^{-2}), and φ is the incident radiative flux (mW cm^{-2}). Photovoltaic performance was measured by using a metal mask with an aperture area of 0.15 cm^2.

The cross section of the device was measured by Zeiss Jemini FEG-SEM, using 5 kV with magnification of 250KX.

Electrical Impedance Measurements (EIS): Impedance measurements were performed by a Bio-Logic SP-300 potentiostat (Bio-Logic SAS, France) over a frequency range from 1 MHz down to 0.1 Hz at forward bias potentials between 0 to 0.6 V (with a 10 mV sinusoidal AC perturbation). The measurements under illumination were performed with a white light LED (LXM3-PW51, Luxeon Rebel, Philips). The resulting impedance spectra were analysed with Z-view software (v2.8b, Scribner Associates Inc.). All Impedance measurements were done in a faradaic cage without mask.

Acknowledgements

This work was supported by Nissan Motor and the ECR advanced grant agreement (No. 247404) under the CE-Mesolight project funded by the European community's 7th FWP.

Received: July 18, 2012
Published online: September 18, 2012

[1] B. O'Reganm, M Grätzel, *Nature* **1991**, *353*, 737.
[2] A. N. M. Green, E. Palomares, S. A. Haque, J. M. Kroon, J. R. Durrant, *J. Phys. Chem. B* **2005**, *109*, 12525.
[3] Y. Aswani, H.-W. Lee, H. N. Tsao, C. Yi, A, K. Chandiran, Md. K. Nazeeruddin, E. W.-G. Diau, M Grätzel, *Science* **2011**, *334*, 629.
[4] N. Cai, S.-J. Moon, L. Cevey-Ha, T. Moehl, R. Humphry-Baker, P. Wang, S. M. Zakeeruddin, M. Grätzel, *Nano Lett.* **2011**, *11*, 1452.
[5] J. Burschka, A. Dualeh, F. Kessler, E. Baranoff, N.-L. Cevey-Ha, C. Yi, M. K. Nazeeruddin, M. Grätzel, *J. Am. Chem. Soc.* **2011**, *133*, 18042.
[6] G. R. R. A. Kumara, A. Konno, G. K. R. Senadeera, P. V. V. Jayaweera, D. B. R. A. De Silva, K. Tennakone, *Sol. Energy Mater. Sol. Cells* **2001**, *69*, 195.
[7] C. Zafer, C. Karapire, N, S. Serdar, S. Icli, *Sol. Energy Mater. Sol. Cells* **2005**, *88*, 11.
[8] G. Larramona, C. Chone, A. Jacob, D. Sakakura, B. Delatouche, D. Pere, X. Cieren, M. Nagino, R. Bayon, *Chem. Mater.* **2006**, *18*, 1688.
[9] L. Etgar, W. Zhang, S. Gabriel, S. G. Hickey, M. K. Nazeeruddin, A. Eychmüller, B. Liu, M. Grätzel, *Adv. Mater.* **2012**, *24*, 2202.
[10] T. Toyoda, J. Sato, Q. Shen, *Rev. Sci. Instrum.* **2003**, *74*, 297.
[11] H. J. Lee, J. H. Yum, H. C. Leventis, S. M. Zakeeruddin, S. A. Haque, P. Chen, S. I. Seok, M. Gratzel, M. K. Nazeeruddin, *J. Phys. Chem. C* **2008**, *112*, 11600.
[12] C. Levy-Clement, R. Tena-Zaera, M. A. Ryan, A. Katty, G. Hodes, *Adv. Mater.* **2005**, *17*, 1512.
[13] O. Niitsoo, S. K. Sarkar, C. Pejoux, S. Ruhle, D. Cahen, G. Hodes, *J. Photochem. Photobiol. A* **2006**, *181*, 306.
[14] L. J. Diguna, Q. Shen, J. Kobayashi, T. Toyoda, *Appl. Phys. Lett.* **2007**, *91*, 023116.
[15] K. Ernst, R. Engelhardt, K. Ellmer, C. Kelch, H. J. Muffler, M. C. Lux-Steiner, R. Konenkamp, *Thin Solid Films* **2001**, *387*, 26.
[16] I. Kaiser, K. Ernst, C. H. Fischer, R. Konenkamp, C. Rost, I. Sieber, M. C. Lux-Steiner, *Sol. Energy Mater. Sol. Cells* **2001**, *67*, 89.
[17] M. Page, O. Niitsoo, Y. Itzhaik, D. Cahen, G. Hodes, *Energy Environ. Sci.* **2009**, *2*, 220.
[18] P. V. Kamat, *J. Phys. Chem. C* **2008**, *112*, 18737.
[19] B. Hanewinkel, A. Knorr, P. Thomas, S. W. Koch, *Phys. Rev.B* **1997**, *55*, 13715.
[20] J. Sun, E. M. Goldys, *J. Phys. Chem. C* **2008**, *112*, 9261.
[21] J. Ah. Chang, J. H. Rhee, S. H. Im, Y. H. Lee, H.-J. Kim, S. I. Seok, M. K. Nazeeruddin, M. Gratzel, *Nano Lett.* **2010**, *10*, 2609.
[22] S. H. Im, H.-J. Kim, J. H. Rhee, C.-S. Lim, S. I. Seok, *Energy Environ. Sci.* **2011**, *4*, 2799.
[23] P. P. Boix, Y. H. Lee, F. Fabregat-Santiago, S. H. Im, I. Mora-Sero, J. Bisquert, S. I. Seok, *ACS Nano* **2012**, *6*, 873.
[24] G. Hodes, *J. Phys. Chem. C* **2008**, *112*, 17778.
[25] Y. Itzhaik, O. Niitsoo, M. Page, G. Hodes, *J. Phys. Chem. C* **2009**, *113*, 4254.
[26] P. P. Boix, G. Larramona, A. Jacob, B. Delatouche, I. Mora-Seró, J. Bisquert, *J. Phys. Chem. C* **2012**, *116*, 1579.
[27] S. Nezu, G. Larramona, C. Choné, A. Jacob, B. Delatouche, D. Péré, C. Moisan, *J. Phys. Chem. C* **2010**, *114*, 6854.
[28] L. G. Ee, M. K. Aik, S. P. Stevin, Y. Natalia, M. Nripan, M. Subodh, *J. Electrochem. Soc.* **2012**, *159*, B247–B250.
[29] M. Y. Versavel, J. A. Haber, *Thin Solid Films* **2007**, *515*, 7171.
[30] H. S. Jung, J. K. Lee, M. Nastasi, S. W. Lee, J. Y. Kim, J. S. Park, K. S. Hong, H. H. Shin, *Langmuir* **2005**, *21*, 10332.
[31] A. Zaban, S. G. Chen, S. Chappel, B. A. Gregg, *Chem. Commun.* **2000**, 2231.
[32] E. Palomares, J. N. Clifford, S. A. Haque, T. Lutz, J. R. Durrant, *J. Am. Chem. Soc.* **2003**, *125*, 475.
[33] P. Wang, L. D. Wang, B. Li, Y. Qiu, *Chin. Phys. Lett.* **2005**, *22*, 2708.
[34] D. B. Menzies, R. Cervini, Y. B. Cheng, G. P. Simon, L. Spiccia, *J. Sol–Gel Sci. Technol.* **2004**, *32*, 363.
[35] S. Nezu, G. Larramona, C. Chon, A. Jacob, *J. Phys. Chem. C* **2010**, *114*, 6854.
[36] Kazuki Tsujimoto, Duy-Cuong Nguyen, Seigo Ito, Hitoshi Nishino, Hiroaki Matsuyoshi, Akinori Konno, G. R. Asoka Kumara, Kirthi Tennakone, *J. Phys. Chem. C* **2012**, *116*, 13465.
[37] P. Wang, S. M. Zakeeruddin, P. Comte, R. Charvet, R. Humphry-Baker, M. Graetzel, *J. Phys. Chem. B* **2003**, *107*, 14336.
[38] P. Wang, S. M. Zakeeruddin, R. Humphry-Baker, J. E. Moser, M. Graetzel, *Adv. Mater.* **2003**, *15*, 2101.
[39] P. Wang, S. M. Zakeeruddin, R. Humphry-Baker, M. Graetzel, *Chem. Mater.* **2004**, *16*, 2694.
[40] Yafit Itzhaki, G. Hodes, H. Cohen, *J. Phys. Chem. Lett.* **2011**, *2*, 2876.
[41] J. Ah. Chang, J. H. Rhee, S. H. Im, Y. H. Lee, H.-J. Kim, S. I. Seok, M. K. Nazeeruddin, M. Gratzel, *Nano Lett.* **2010**, *10*, 2609.
[42] Z. Zhang, N. Evans, S. M. Zakeeruddin, R. Humphry-Baker, M. Grätzel, *J. Phys. Chem. C* **2006**, *111*, 398.
[43] S. J. Moon, J. H. Yum, R. Humphry-Baker, K. M. Karlsson, D. P. Hagberg, T. Marinado, A. Hagfeldt, L. C. Sun, M. Grätzel, M. K. Nazeeruddin, *J. Phys. Chem. C* **2009**, *113*, 16816.
[44] S. Messina, M. T. S. Nair, P. K. Nair, *Thin Solid Films* **2007**, *515*, 5777.
[45] J. Ah. Chang, J. H. Rhee, S. H. Im, Y. H. Lee, H.-J. Kim, S. I. Seok, M. K. Nazeeruddin, M. Gratzel, *Nano Lett.* **2010**, *10*, 2609.